



Study of tungsten oxide effect on the performance of BaTiO₃ ceramics

Y. Slimani¹ · A. Selmi² · E. Hannachi³ · M. A. Almessiere^{1,4} · M. Mumtaz⁵ · A. Baykal⁶ · I. Ercan¹

Received: 28 March 2019 / Accepted: 19 June 2019 / Published online: 26 June 2019
© Springer Science+Business Media, LLC, part of Springer Nature 2019

Abstract

BaTiO₃/(WO₃)_x ceramics (where x = 0, 0.5, 1, 2 and 5 wt%) were prepared by solid state reaction. X-ray powder diffraction, scanning electron microscope, Fourier transform-infrared spectroscopy and ultraviolet–visible diffuse reflectance spectrophotometry were used to investigate the structure, morphology and optical properties, respectively. The electrical and dielectric properties were also performed for different synthesized ceramics. A pure phase was obtained for x = 0.5 wt% ceramic, nevertheless a secondary phase was detected for x ≥ 1 wt% ceramics. The grains size increases for x = 0.5 wt% ceramic and then reduces abruptly with further increasing WO₃ content. The increase of grains size and the absence of impurities were all efficient to enhance the dielectric properties. A suitable WO₃ content leads to obtain ceramics having high dielectric constant and low tangent loss, which is encouraging for radio frequencies and microwaves applications.

1 Introduction

Due to their ferroelectric, piezoelectric, photoelectric, dielectric, pyroelectric and catalytic responses, the perovskite oxides having ABO₃ structure has attracted a great attention [1–3]. These properties lead them to be used in various

applications including electro-optical and electronics. One of the most common ferroelectric material is BaTiO₃ (barium titanate; noted BTO) that exhibits important dielectric constant and resistivity and a low dielectric loss. BTO has a tetragonal ferroelectric structure at room temperature (RT) with lattice parameters a = 3.994 Å and c = 4.034 Å [4, 5]. This material is extensively used for electronic devices such as storage devices, capacitors, thermistors, piezoelectric transducers, sensors, etc. [6, 7]. The synthesis of nanosized BTO can be realized through numerous routes, including hydrothermal method, sol–gel process, solid-state reaction method, chemical coprecipitation, etc. [8].

To be performant in the various mentioned applications, it is necessary to control the microstructure of such material. The dielectric properties could be altered by adding dopants. Many types of additives have been included to perovskites ceramics and influenced their dielectric properties. Previous works have been done on BTO-SiO₂ [9–16]. Luo [13] have explored the impact of SiO₂ on the microstructural and dielectric properties of BTO product prepared by microwave sintering method. It was found that an optimal SiO₂ content lead to improve the dielectric properties of BTO, particularly the permittivity increased and the dielectric loss decreased. Bi et al. [14] produced ultrafine nanostructures of BTO@SiO₂ core–shell. Experimental results showed an optimization of the microstructure and dielectric responses. Furthermore, the ultrafine nanostructures provide high polarization that could efficiently enhance the electrical displacement and the breakdown strength simultaneously. The researchers

✉ Y. Slimani
yaslimani@iau.edu.sa; slimaniyassine18@gmail.com

✉ E. Hannachi
hannechi.essia@gmail.com

¹ Department of Physics Research, Institute for Research & Medical Consultations (IRMC), Imam Abdulrahman Bin Faisal University, P.O. Box 1982, Dammam 31441, Saudi Arabia

² Laboratoire Matériaux Organisation et Propriétés (LMOP), Université de Tunis El Manar, Campus Universitaire, 2092 El Manar, Tunis, Tunisia

³ Laboratory of Physics of Materials - Structures and Properties, Department of Physics, Faculty of Sciences of Bizerte, University of Carthage, 7021 Zarzouna, Tunisia

⁴ Department of Physics, College of Science, Imam Abdulrahman Bin Faisal University, P.O. Box 1982, Dammam 31441, Saudi Arabia

⁵ Materials Research Laboratory, Department of Physics, FBAS, International Islamic University (IIU), Islamabad 44000, Pakistan

⁶ Department of Nano-Medicine Research, Institute for Research & Medical Consultations (IRMC), Imam Abdulrahman Bin Faisal University, P.O. Box 1982, Dammam 31441, Saudi Arabia

confirmed the advantage of the ultrafine structures in improving the energy density of these ceramics, which provide an innovative technological method for the fabrication of high energy–density ceramics. Contrarily, Yan et al. [15] synthesized SiO₂ added BaTiO₃ ceramics and they found that with increasing the SiO₂ content, an impurity phase was detected. This leads to decrease gradually the dielectric constant however an improvement of the electrical breakdown strengths was noticed. Furthermore, Lu et al. [16] synthesized series BTO-SiO₂ composites through a combined route of conventional ceramic method and wet chemical coating. It is observed also a decrease of the dielectric constant on increasing the SiO₂ content. BTO particles coated with Al₂O₃ were synthesized by Zhao et al. [17]. It is showed that the coating with Al₂O₃ leads to reduce the grains size and to narrow distribution. Furthermore, the synthesized products with Al₂O₃ coating showed an enhancement of dielectric properties, breakdown strength, energy efficiency and discharge energy density at room temperature compared to that produced without Al₂O₃ coating. Several groups synthesized BaTiO₃-TiO₂ ceramics for dye-sensitized solar cell applications [18–22]. An improvement in the photoelectronic conversion efficiency (PCE) and charge carrier separation ability of the composites was attained. This provides that the BaTiO₃-TiO₂ ceramics could be considered as promising for photocatalytic activity and photovoltaic systems. Paunović et al. [23] investigated the effects of rare-earth (RE = Dy, Sm and La) additions on the microstructural and dielectric properties of BTO ceramics. A low doping additive reveals an improvement of dielectric permittivity value together with low dissipation factor at RT. The impact of NiO inclusion on the microstructural and electrical properties of BTO was studied [24]. It is showed that NiO additions reduces the relative permittivity and temperature sensitivity of the doped BTO ceramics. Numerous other doping in BTO ceramics were reported in previous studies, such as MgO [25], CaO [26], Y₂O₃ [27], Cu [28], Sr-Ca [29] and RE = Lu, Yb, Er, Ho, Dy, Tb, Gd, Pr, La, Eu [30, 31] doped BaTiO₃.

Particularly, as a transition metal oxide (TMO), the tungsten oxide (WO₃) is widely exploited in diverse technological applications such as optical recording devices, photocatalytics, sensors and electro-chromic devices [32, 33]. WO₃, n-type semiconductor, is the most promising TMO that display electrochromic behavior in the infrared and visible region and exhibit better electrical properties and optical modulation regarding the other TMO [34]. Besides, WO₃ possesses the performance of ferroelectric materials, yielding it to be utilized in numerous fields including anti-dazing devices, air condition, house building solar energy, automotive glasses, and smart windows [34]. Recently, thin films of WO₃ have been explored for their sensing properties [35]. The former properties will lead to various applications in industrial pollution monitoring and environmental.

Very recent, Slimani et al. [36, 37] investigated the influences of nano-sized WO₃ entities on the performances of high-temperature YBa₂Cu₃O_y superconductor. The obtained results revealed an improvements in electrical and magnetic properties, particularly critical current densities, flux pinning capacities and critical magnetic fields. It is concluded that the inclusion of appropriate content of WO₃ nanoentities into the high-temperature superconductor materials is an efficient route for improving their performances. Up today, the utilization of WO₃ as additive in the BTO ceramics has not been yet studied in the literature. Accordingly, it is very important to investigate the influences of various WO₃ amounts on the dielectric properties of BTO material. Therefore, series of BaTiO₃/(WO₃)_x ceramics, where x = 0, 0.5, 1, 2 and 5 wt%, were prepared. The effect of various WO₃ contents inclusion on the structure, morphology, spectral, optical and dielectric properties of BTO-based products was deeply discussed.

2 Experimental

2.1 Materials and instrumentations

High purity (99.99%) powders of BaCO₃, TiO₂ and WO₃ were obtained from Sigma Aldrich. The planetary Ball Mill PM 200 from Retsch was employed to grind samples. X-ray powder diffraction (XRD; Rigaku Benchtop Miniflex) with Cu-K α radiation was used to examine the phase identification. Bruker alpha-II FT-IR spectrometer was employed to perform Fourier transform-infrared (FT-IR) spectra. The morphological observation was done by FEI Quanta FEG scanning electron microscope (SEM). UV-Vis spectrophotometer (JASCO V-780) was used to collect the diffuse reflectance spectra (DRS). The dielectric and electrical measurements were carried out by means of Alpha-N high-resolution analyzer from Novocontrol Technologies.

2.2 Synthesis

Various series of BaTiO₃/(WO₃)_x ceramics, where x = 0, 0.5, 1, 2 and 5 wt% were prepared via solid state reaction by using high energy ball milling (HEBM). The different powders were mixed stoichiometrically with respect to the desired compositions in ethanol. After, the mixtures were ball-milled in the planetary HEBM as a grinding media for 14 h. After drying, the grinded powders were pressed into discs with 13 mm in diameter. The obtained pellets were calcined at 1100 °C for 12 h. The steps of ball-milling, pressing into discs and calcination were repeated twice in order to achieve the desired nano-sized composites.

3 Results and discussion

3.1 Structural analysis

XRD patterns of the synthesized BaTiO₃/(WO₃)_x ceramics shown in Fig. 1 are analyzed using Match program

in order to determine the different structural parameters. The deduced phase fractions and lattice parameters are listed in Table 1. The goodness of the fit was evaluated through the Bragg R_B factor and χ² (Table 1). The data of pure BTO sample is found to match very well with the tetragonal phase (ICCD no. 96-210-0860) and space group P4mm. Figure 2 shows an enlarged view of the (002) and

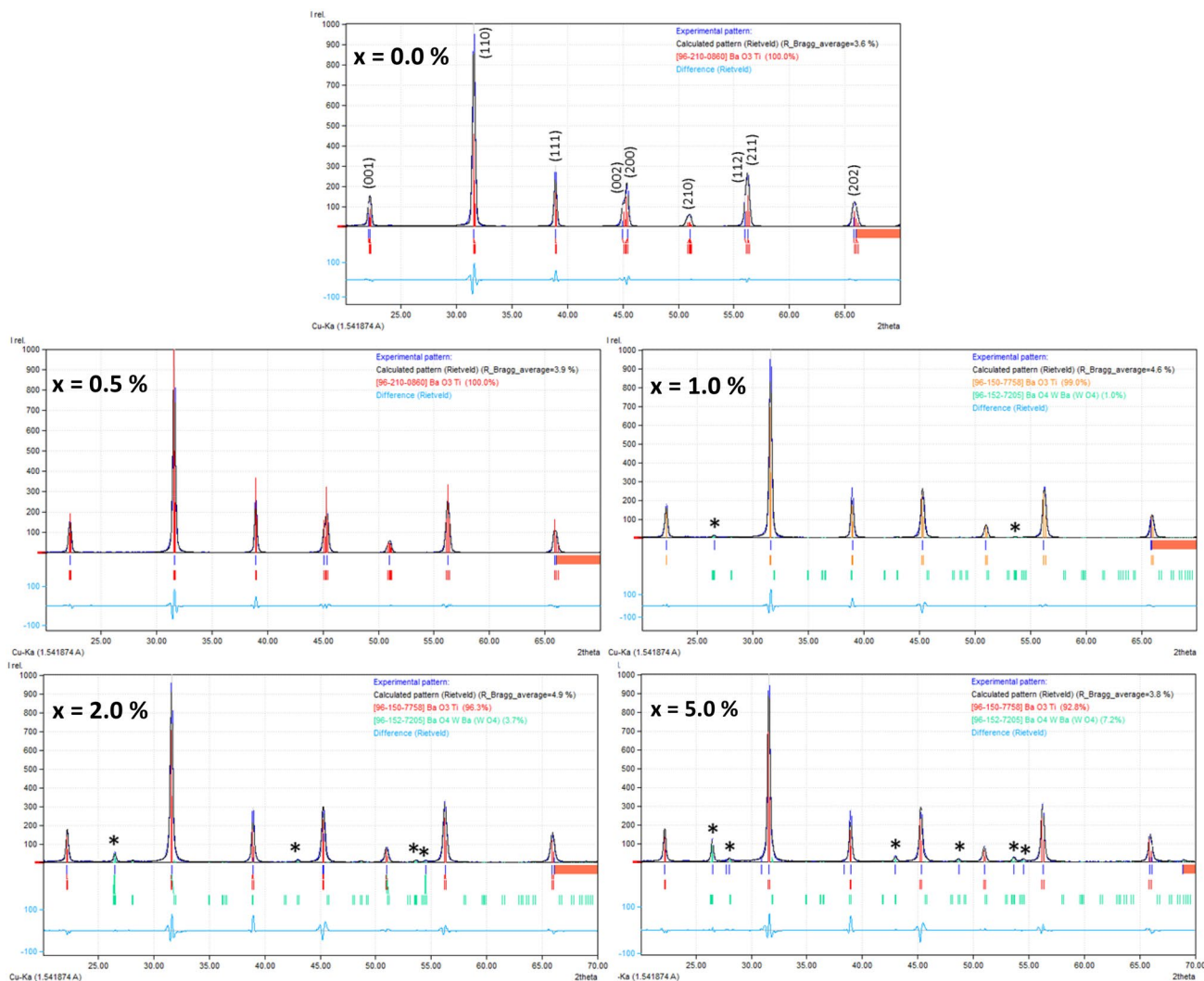


Fig. 1 Rietveld refinement of XRD patterns of various BaTiO₃/(WO₃)_x ceramics. The asterisk (*) corresponds to the BaWO₄ impurity

Table 1 Phase fractions, structural parameters, crystallites size and densities of various BaTiO₃/(WO₃)_x composites

| x content (%) | Phase fractions (%) | | Lattice parameters | | c/a | R _B | χ ² | D _{XRD} (nm) | Density (g/cm ³) |
|---------------|---------------------|----------|--------------------|--------|--------|----------------|----------------|-----------------------|------------------------------|
| | BaTiO ₃ | Impurity | a=b (Å) | c (Å) | | | | | |
| 0.0 | 100 | – | 3.9987 | 4.0283 | 1.0074 | 3.6 | 1.9 | 64.71 | 4.96 |
| 0.5 | 100 | – | 3.9982 | 4.0276 | 1.0073 | 3.9 | 1.1 | 78.14 | 5.47 |
| 1.0 | 99.0 | 1.0 | 4.0062 | – | 1.0000 | 4.6 | 1.2 | 55.82 | 4.22 |
| 2.0 | 96.3 | 3.7 | 4.0055 | – | 1.0000 | 4.9 | 0.8 | 51.27 | 4.05 |
| 5.0 | 92.8 | 7.2 | 4.0052 | – | 1.0000 | 3.8 | 0.8 | 51.42 | 3.96 |

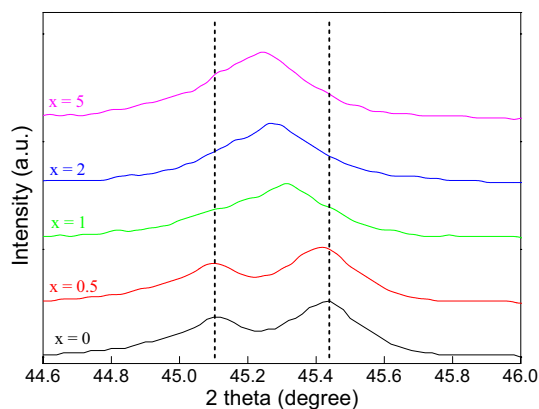


Fig. 2 Enlarged view of the (002) and (200) reflection peaks for various $\text{BaTiO}_3/(\text{WO}_3)_x$ ceramics

(200) reflection peaks. The presence of splitting in (002)/(200) reflections for $x=0.0$ and 0.5 samples is an indication of the tetragonal structure [38]. The lattice parameters $a=b=3.9987 \text{ \AA}$ and $c=4.0283$ for pristine BTO product and its $c/a=1.0074$ ratio are thoroughly comparable to those reported in the literature [38, 39]. As seen from Table 1, a and c decrease slightly with small WO_3 content addition (i.e. $x=0.5\%$). This is mostly ascribed to the doping of W ions having ionic radii of 0.6 \AA , which is smaller than those of Ba^{2+} (1.61 \AA) and Ti^{4+} (0.62 \AA) ions. The c/a ratio is almost constant for $x=0.0$ ($c/a=1.0074$) and $x=0.5$ ($c/a=1.0073$) ceramics. The decrease in the tetragonality of the structure could be approved by investigating the splitting of the (200) and (002) peaks. Nevertheless, the $x=0.5$ ceramic exhibit well-split (200)/(002) peaks, confirming that the tetragonality was maintained for low doping content. The c/a ratio for $x \geq 1$ wt% samples is equal to 1, indicating the cubic structure (ICCD no. 96-150-7758) with $Pm3m$ space group in these products. This can be confirmed by the vanishing of the peak (002) plane in $x \geq 1$ wt% samples, which is already exist in pure BTO sample along with the peak of (200) plane [40]. The merging of the two (002)/(200) reflections is a clear indication of the cubic structure.

Both $x=0.0$ and 0.5 samples does not contain any impurity. Nevertheless, BaWO_4 secondary phase (marked as ‘*’; ICCD no. 96-152-7205) begins to appear for $x \geq 1$ wt%. The concentration of impurity phase increases remarkably with rising the WO_3 content. The densities were determined and values are listed in Table 1. With increasing WO_3 doping content from 0.0 to 0.5 wt%, the density increased from 4.96 to 5.47 g/cm^3 . The addition of WO_3 with lower content was found to be very helpful for the densification of BTO. The enhancement of densification of $x=0.5$ wt% ceramic could contribute to further enhanced dielectric and electrical properties.

Nevertheless, with further increasing WO_3 content (i.e. $x \geq 1$ wt%), the density decreased continuously. That is mostly due to presence of BaWO_4 secondary phase [15]. The average crystallites size (D_{XRD}) is estimated for all synthesized ceramics by using Scherrer equation [41]:

$$D_{\text{XRD}} = \frac{k\lambda}{\beta \cos\theta} \quad (1)$$

where k is a constant close to unity ($k=0.9$), $\lambda=1.5418 \text{ \AA}$ for Cu $K\alpha$ radiations, θ is Bragg’s angle and β is full width at half maximum. The estimated D_{XRD} values for various $\text{BaTiO}_3/(\text{WO}_3)_x$ ceramics are listed in the Table 1 and are found to be in the range of 78.14 – 51.27 nm. It is obvious that the D_{XRD} increases firstly for $x=0.5$ wt% and then diminishes as the WO_3 content increase. In previous investigations, it is reported that the tetragonality of the products reduces with reducing the grains size and can attain the cubic structure [42, 43]. This accords with the present obtained findings in which both the D_{XRD} and tetragonality decrease with increasing WO_3 doping content.

3.2 Morphological examination

SEM micrographs of $\text{BaTiO}_3/(\text{WO}_3)_x$ ceramics are showed in Fig. 3. Pure BTO (Fig. 2a) demonstrated a morphology with homogeneous nano-sized grains. Compared to pure sample, the grains size increase for lower WO_3 doping content (i.e. $x=0.5$). As seen from Fig. 3b–d, the samples with WO_3 doping showed similar microstructures with pure BTO product, but with smaller grains size. The grains size decreases gradually with increasing WO_3 doping content. This involves that the sintering temperatures of ceramics is decreased with the WO_3 addition [15].

3.3 FT-IR investigation

The FT-IR spectra of the prepared $\text{BaTiO}_3/(\text{WO}_3)_x$ ceramics are showed in Fig. 4. All the products revealed characteristic band at about 500 cm^{-1} which correspond to the Ti–O vibration [44]. Another characteristic band with small intensity is observed around 1450 cm^{-1} for all composites, which is mostly attributed to the Ba–Ti–O vibration [44]. Except these two characteristic bands, a change is noticed in the composites prepared with high x content. In fact, an additional characteristic band is appeared between 820 and 850 cm^{-1} for the two composites synthesized with $x=2$ and 5 . This band is most probably a result of the signals of the W–O stretching vibration [45]. The intensity of this typical peak is higher in $x=2$ wt% composite compared to $x=5$ wt%. The FT-IR results prove the formation of the desired $\text{BaTiO}_3/(\text{WO}_3)_x$ ceramics.

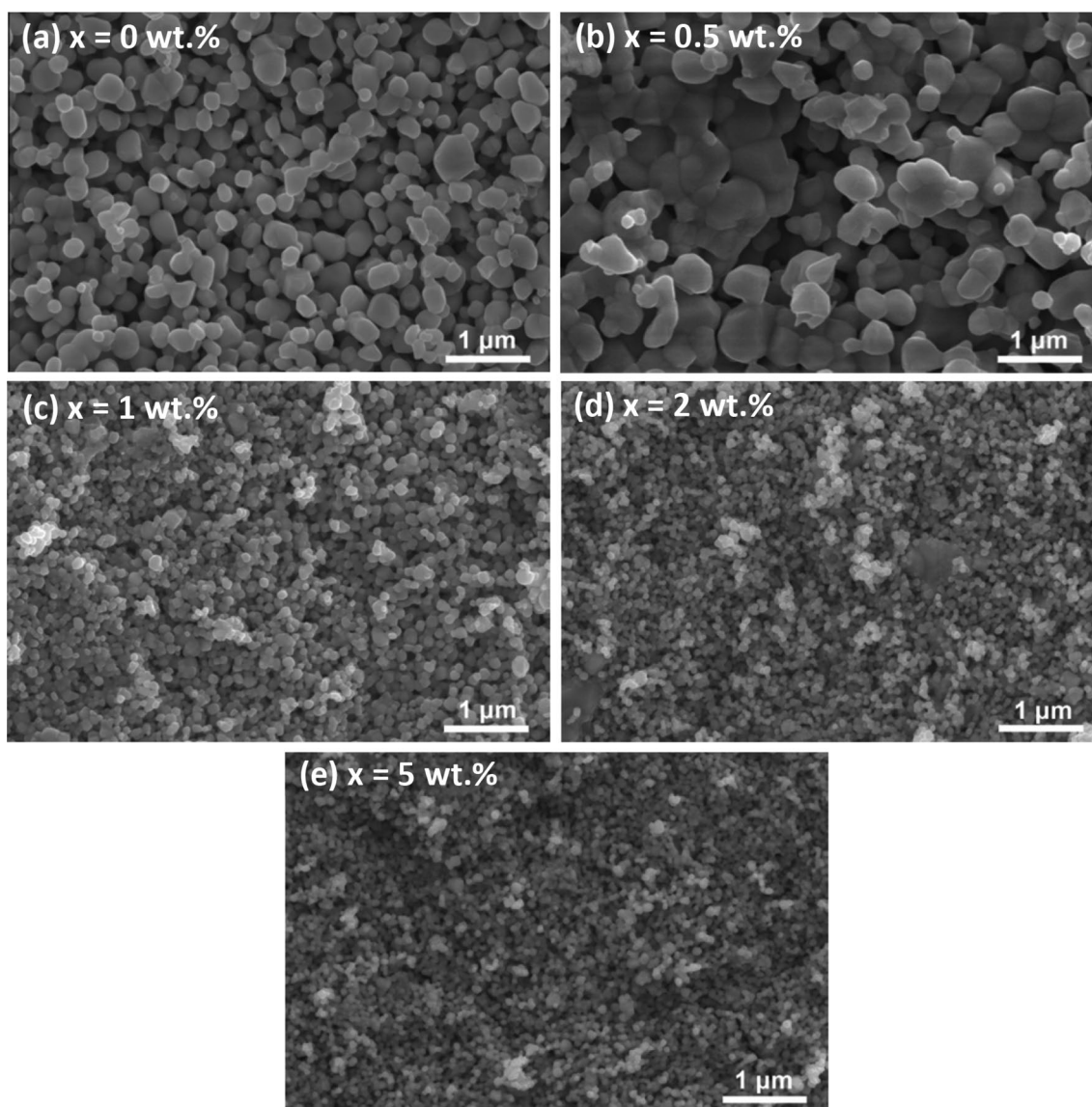


Fig. 3 SEM micrographs of the synthesized $\text{BaTiO}_3/(\text{WO}_3)_x$ ceramics where **a** $x=0$, **b** $x=0.5$, **c** $x=1$, **d** $x=2$ and **e** $x=5$ wt%

3.4 Optical investigation

The UV–Visible DRS analysis was utilized to explore the optical properties of $\text{BaTiO}_3/(\text{WO}_3)_x$ ceramics. When a matter is irradiated by a light beam, it is known that the incident light will be reflected, transmitted and/or scattered inside the matter. Generally, the beam part that will scatter inside the matter and return to the surface is known as the diffused reflectance. Figure 5 presents the UV–Vis DRS of various synthesized $\text{BaTiO}_3/(\text{WO}_3)_x$ ceramics in the range of 200–800 nm. The spectra revealed an absorption of around 80% of light for various $\text{BaTiO}_3/(\text{WO}_3)_x$ ceramics in the UV range. Tauc model was employed to deduce the optical band gap energy (E_g) according to the following expression [46, 47]:

$$\alpha h\nu = \alpha (h\nu - E_g)^r \quad (2)$$

where $h\nu$ is the photon energy and α is a constant independent on photon energy. The exponent r display four numeric values: $r=3/2$ for forbidden indirect, $r=2$ for allowed indirect, $r=3$ for forbidden direct, and $r=1/2$ for allowed direct optical transitions. Since BTO has a direct band gap [48], hence by plotting $(\alpha h\nu)^2$ as a function of $h\nu$, its E_g can be deduced. The direct band gap is deduced by extrapolating the linear portion to the low energies. The E_g values of $\text{BaTiO}_3/(\text{WO}_3)_x$ ceramics is deduced from the UV–Visible DRS by converting the diffused reflectance (R) values according to the Kubelka–Munk equation [46, 47]:

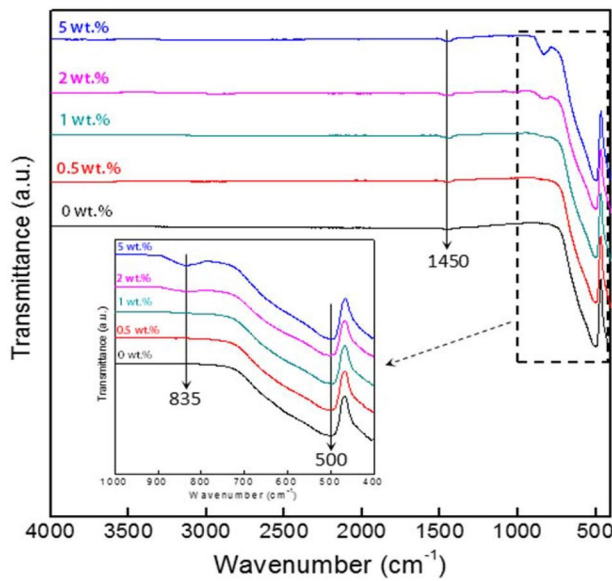


Fig. 4 FT-IR spectra of different prepared $\text{BaTiO}_3/(\text{WO}_3)_x$ ceramics where $x=0, 0.5, 1, 2$ and 5 wt%

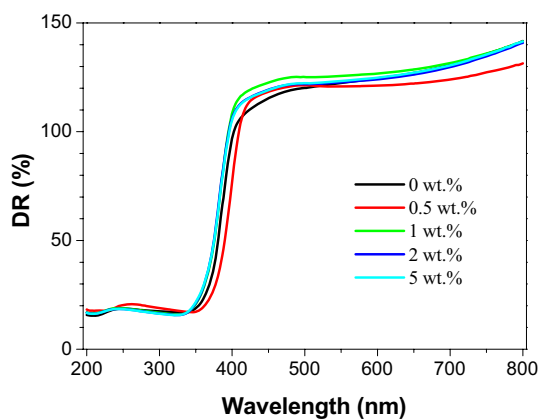


Fig. 5 DRS spectra of various prepared $\text{BaTiO}_3/(\text{WO}_3)_x$ ceramics

$$F(R) = \alpha = \frac{(1-R)^2}{R} \quad (3)$$

Figure 6 presents plots of $(\alpha h\nu)^2$ against $h\nu$. The values of E_g of various prepared ceramics were deduced by extrapolating the linear portions as presented in the inset of Fig. 6. The pristine BTO sample display E_g value of about 3.31 eV. The obtained value is lower than that of bulk BTO ($E_g = 3.23$ eV [49]) because of quantum size effect. The E_g values for 0.5, 1, 2 and 5 wt% ceramics were found to be equal to 3.24, 3.38, 3.41 and 3.42 eV, respectively. Compared to $x=0$ wt% sample, a reduction of E_g from 3.31 to 3.24 eV was noticed in 0.5 wt% ceramic. The reduction of E_g in this ceramic could be ascribed to the increase in grains size and crystallinity as shown above in XRD and SEM analyses [50]. For

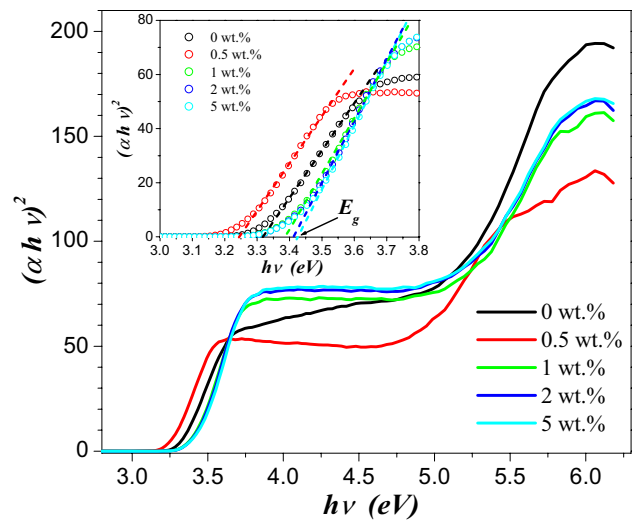


Fig. 6 Tauc plots of the different synthesized $\text{BaTiO}_3/(\text{WO}_3)_x$ ceramics. The inset showed an enlarged view to estimate the energy band gaps

ceramics with $x \geq 1$ wt%, the E_g values show an increase, which might be accredited to the reduction in grains size. Furthermore, the dependence of E_g on the grains size may be described using the electron confinement effect. When the particles size is being smaller, quantum confinement effect will occur and the motion of electrons will be confined in discrete states, which led to an increase in the band gap energy [50, 51]. Another possible reason for the change in E_g values is the presence of BaWO_4 impurities in the $\text{BaTiO}_3/(\text{WO}_3)_x$ ceramics [52].

3.5 Dielectric and electrical properties

3.5.1 Dielectric studies

The loss tangent ($\text{tg}\delta$) and dielectric permittivity (ϵ') responses versus frequency (10 Hz to 10 MHz) of the various $\text{BaTiO}_3/(\text{WO}_3)_x$ ceramics at RT are presented in Figs. 7a and b, respectively. It can be observed that the dielectric constant ϵ' of all ceramics reduces on increasing the frequency and reaches a constant magnitude at higher frequencies, exhibiting dispersion behavior. The reduction of ϵ' at lower frequencies originates from the polarization effect that does not happen immediately on applying the electric field due to inertia. The dipoles that are induced will follow the electric field at very low frequencies, and fully participate to the total polarization of the dielectric. At higher frequency, the dipoles are not able to align themselves due to very rapid variations in the field. As consequence, their influence on the polarization as well as on the ϵ' become insignificant [53]. The observed high values of ϵ' at lower frequency for all ceramics could be attributed to charges accumulation within grain

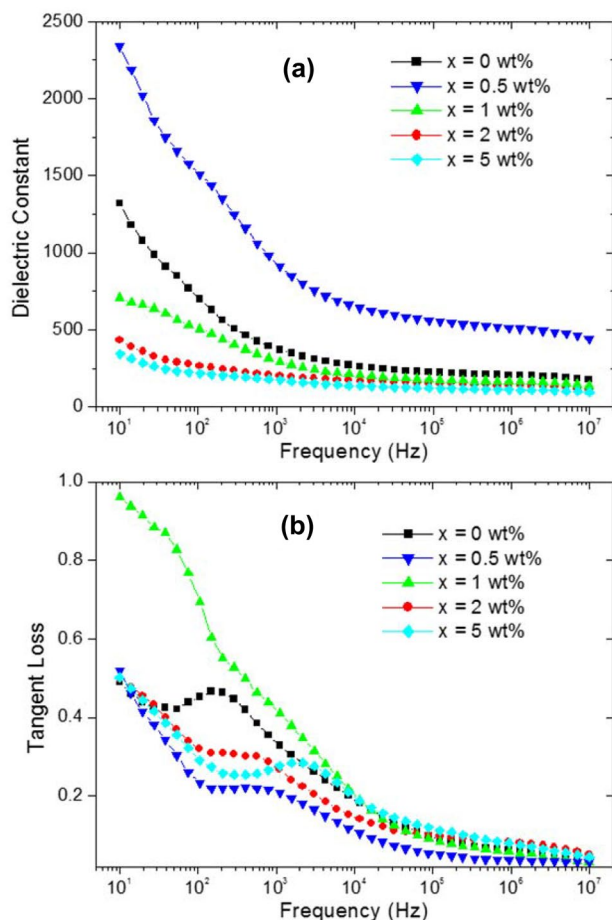


Fig. 7 a Frequency dependence of the dielectric constant ϵ' and b loss tangent ($\tan \delta$) of the BaTiO₃/(WO₃)_x ceramics with different volume fraction of x = 0, 0.5, 1, 2 and 5 wt%

boundaries, and at the interfaces among the electrode and the sample, i.e. Maxwell–Wagner polarization and interfacial polarization [54]. As seen in Fig. 7b, the dispersion behavior observed in dielectric permittivity is followed by a peak of relaxation in loss tangent ($\tan \delta$). The position of the $\tan \delta$ peak shifts to higher frequencies with increasing the WO₃ content. The dependence of loss peak on frequency indicates that the charge carriers hopping has a significant impact on their transport processes [55]. At high frequencies ($f > 10$ kHz), the losses show a decrease for all ceramics, which is encouraging for microwaves and radio frequencies applications.

The dielectric properties strongly depended on the WO₃ concentration (see Figs. 7 and 8). Firstly, with increasing WO₃ concentration from 0.0 to 0.5 wt%, the dielectric constant shows a significant improvement. This change in permittivity may be attributed to the microstructure of x = 0.5 ceramic. The increase of ϵ' could be described by the improvement of the microstructure. In fact, the addition of WO₃ can increase the grain size and subsequently the dielectric permittivity. Several authors have shown that the ϵ'

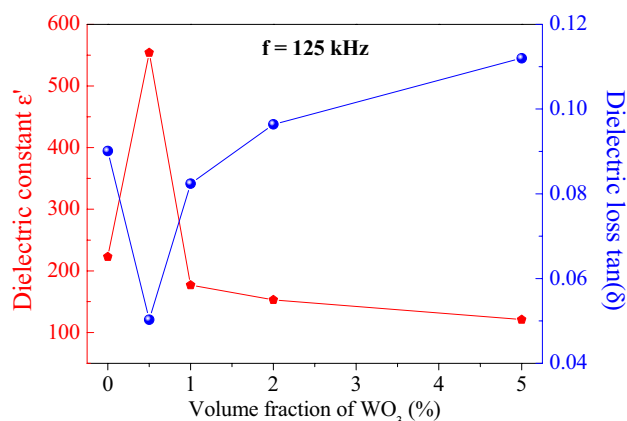


Fig. 8 Dielectric permittivity and dissipation factor of the BTO ceramics as function of WO₃ volume fraction at 125 kHz

increases with grains size [55, 56]. In addition, the increase of ϵ' is mostly qualified to the WO₃ doping effect. The increase of doping content could strengthen the interaction among adjacent dipoles, which is beneficial to obtain high dielectric constant [57]. With further increasing the concentration of WO₃, the dielectric permittivity shows a strong decrease. This change in permittivity with the increase of the doped concentration is not surprising and can be attributed to the microstructure of ceramics with $x \geq 1$ wt%. Indeed, in agreement with the SEM images, the ceramic products with $x \geq 1$ wt% show smaller grains size in comparison with the pure BTO and x = 0.5 samples. Moreover, the highly possible substitution of larger number of Ti⁴⁺ ions by W⁴⁺ (due to nearest ionic radii) could lead to narrowing the space between oxygen octahedrons and lowering the spontaneous polarization, or even partially losing the ferroelectricity, ultimately conducting to a reduction in ϵ' [57]. Furthermore, the excessive increase of non-ferroelectric secondary phases can weak the dielectric constant [57]. Higher inclusion of WO₃ resulted in a microstructure consisting of two-phases (see XRD results), and therefore, the ϵ' of the ceramics reduces with rising WO₃ content above 1 wt%. For $x \geq 1$ wt%, the variations in the crystallinity provoked by W⁴⁺ ions along with changes of the grains size have larger influences on the dielectric constant [56]. Therefore, the x = 0.5 wt% with greater crystallinity, bigger grains size and absence of non-ferroelectric secondary phases has the maximum ϵ' value. The dielectric loss ($\tan \delta$) is also strongly influenced by the WO₃ doping concentration and is very related to the sample microstructure and presence/absence of secondary phases.

The x = 0.5 wt% ceramic exhibits the maximum permittivity and the lowest dielectric loss ($\tan \delta$) at RT, indicating that it is more suitable for use in tunable devices at RT. The dielectric and ferroelectric properties at microwave frequencies and in a broad range of temperature of $x \leq 0.5$ products will be described in detail in a future article.

3.5.2 Electrical conductivity investigation

Using dielectric data, the ac electrical conductivity (σ_{ac}) of $\text{BaTiO}_3/(\text{WO}_3)_x$ ceramics was calculated using the empirical formula:

$$\sigma_{ac} = \omega \varepsilon' \varepsilon_0 \tan(\delta) \quad (4)$$

ε_0 is vacuum permittivity and $\omega = 2\pi f$ is angular frequency. Figure 9 displays the frequency variation of σ_{ac} for diverse synthesized $\text{BaTiO}_3/(\text{WO}_3)_x$ ceramics where $x = 0, 0.5, 1, 2$ and 5 wt%. The study of the conductivity in alternative regime shows the same pace for all the samples; σ_{ac} rises as the frequency increases due to the increment in carriers charge hopping. To explain its behavior, the σ_{ac} data was evaluated by the Jonscher's power law of the universal dielectric response model [58]:

$$\sigma_{ac} = \sigma_{dc} + A\omega^n \quad (5)$$

Here A is a pre-exponential constant, σ_{dc} is the dc bulk conductivity, and n is the power-law exponent varying between 0 and 1. Generally, for perovskite oxides, there are two conductivity behaviors:

- (i) Low frequency region, in which the conductivity is almost independent on frequency (called σ_{dc}), the charge carriers make jumps long distance through the volume of the material to the electrodes.
- (ii) High frequencies region, where conductivity is frequency dependent and show a linear behavior. In this regime, the charge carriers trapped at the grain boundaries make short jumps. The conduction process is therefore related to a dielectric relaxation mechanism.

In our work, we observe that the dc conductivity behavior is not very clear and it can be visible for frequencies

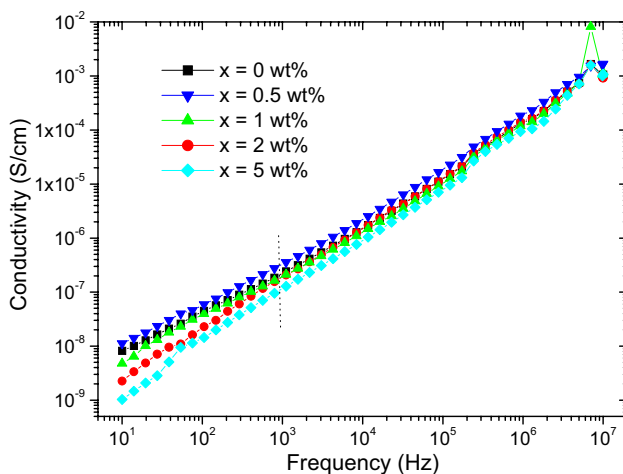


Fig. 9 Frequency dependence of the electrical conductivity (σ_{ac}) of the $\text{BaTiO}_3/(\text{WO}_3)_x$ ceramics where $x = 0, 0.5, 1, 2$ and 5 wt%

lower than 1 kHz, by against the asymptotic regime ($A\omega^n$) is dominant. This suggests that the short-range motions of carriers govern the relaxation processes. The conductivity remains almost the same for all the concentrations of WO_3 at high frequency, while a slight difference in conductivity is obtained at low frequency. Finally, the high ε' , low $\tan \delta$, and low σ of the prepared ceramics make them promising candidates to be used in embedded devices in the micro-electronics industry.

3.5.3 Electrical modulus analysis

For the composite structure, it is always better to know the effect of each phase (i.e., the dissociation between the bulk and the interface effect) and to highlight the effect of adding. The electric modulus (M^*) could give important details about the relaxation mechanism. This formalism has the benefit of suppressing the polarization of electrodes and phenomena of space charge injection and identify the effects of grains and grain boundaries contributions on the charge transport in the poly-crystalline compounds [59, 60]. Based on the complex permittivity $\varepsilon^* = \varepsilon' - j\varepsilon''$, M^* can be expressed as follow:

$$M^* = M' + jM'' \quad (6)$$

$$M' = \frac{\varepsilon'}{(\varepsilon'^2 + \varepsilon''^2)} \quad (7)$$

$$M'' = \frac{\varepsilon''}{(\varepsilon'^2 + \varepsilon''^2)} \quad (8)$$

where M' and M'' are the real and imaginary components of the M^* , respectively.

Figure 10 depicts the imaginary part (M'') versus the real part (M') of the electrical modulus over the same frequency range for different prepared $\text{BaTiO}_3/(\text{WO}_3)_x$ ceramics. The figure shows a clear effect of WO_3 doping on the electric modulus behavior. It is clear seen that the pure BTO and $x = 0.5$ ceramics show only one semi-circle, while the ceramics prepared with $x \geq 1$ wt% exhibit two semi-circles. This behavior suggests that the ceramics with $x \geq 1$ wt% are composed of two phases. The representation of the imaginary part versus the real part of the electrical modulus at RT of the $x \geq 1$ wt% ceramics shows the presence of two partially overlapping semi-circles. This behavior is occurred when the materials present a dual effect: the bulk and the interfacial effect. More clearly, the semi-circle observed at lower frequency is attributed to the interfacial effect specified by the interface between the BaTiO_3 matrix and the WO_3 nanoparticles, while the semi-circle occurred at higher frequency is due to the BaTiO_3 -bulk effect.

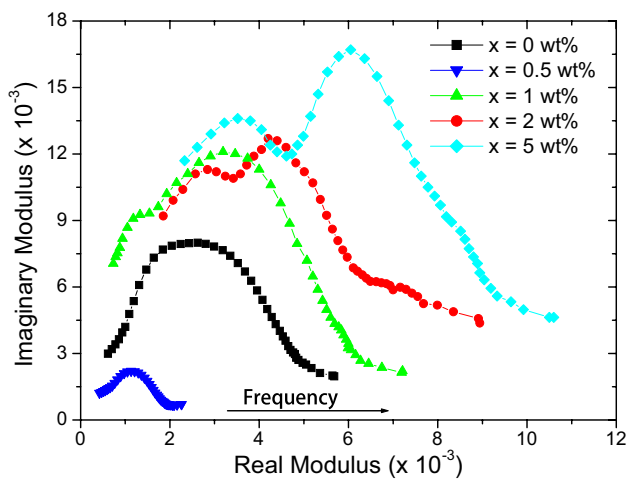


Fig. 10 Variation of imaginary part (M'') of electrical modulus versus real part (M') at room temperature for various $\text{BaTiO}_3/(\text{WO}_3)_x$ ceramics

4 Conclusion

In this investigation, $\text{BaTiO}_3/(\text{WO}_3)_x$ ceramics (where $x=0, 0.5, 1, 2$ and 5 wt%) were successfully prepared via solid state reaction route. According to XRD analysis, pristine compound (i.e. $x=0$ wt%) showed pure BTO phase with tetragonal structure. When WO_3 content is 0.5 wt%, no impurity was observed, and it exhibited larger grains size with homogeneous microstructure compared to pristine product. Nevertheless, when $x \geq 1$ wt%, appearance of BaWO_4 secondary phase, tetragonal-cubic structure transition and a reduction in grains size were noticed. A variation in E_g was remarked with WO_3 additions in BTO, which might be ascribed to variations of grains size and existence of impurities. The investigation of electrical and dielectric properties indicated that $x=0.5$ wt% ceramic exhibit great dielectric constant and low tangent loss. The obtained results are encouraging to use the obtained ceramic in radio frequencies and microwaves applications.

Acknowledgements This work was supported by the Institute for Research & Medical Consultations (Projects Nos. 2017-IRMC-S-3 and 2018-IRMC-S-2) and the Deanship for Scientific Research (Projects Nos. 2018-209-IRMC and 2017-576-IRMC) of Imam Abdulrahman Bin Faisal University (IAU – Saudi Arabia).

References

- C.D. Chandler, C. Roger, M.J. Hampden-Smith, Chemical aspects of solution routes to perovskite-phase mixed-metal. *Chem. Rev.* **93**, 1205–1241 (1993)
- M.A. Pena, J.L.G. Fierro, Chemical structures and performance of perovskite oxides. *Chem. Rev.* **101**, 1981–2017 (2001)
- S. Royer, D. Duprez, F. Can, X. Courtois, C. Batiot-Dupeyrat, S. Laassiri, H. Alamdari, Perovskites as substitutes of noble metals for heterogeneous catalysis: dream or reality. *Chem. Rev.* **114**, 10292–10368 (2014)
- H.F. Kay, H.J. Vellard, P. Vousden, Atomic positions and optical properties of barium titanate. *Nature* **163**, 636 (1949)
- J. Harada, T. Pedersen, Z. Barnea, X-ray and neutron diffraction study of tetragonal barium titanate. *Acta Cryst. B* **26**, 336 (1970)
- M. Wongduan, K. Reinhard, B.H. Robert, P. Simon, Structural and dielectric properties of $\text{Ba}_{0.8}\text{La}_{0.133}\text{Ti}_{0.90}\text{Sn}_{0.1}\text{O}_3$. *J. Eur. Ceram. Soc.* **23**, 127 (2003)
- M.Z.-C. Hu, G.A. Miller, E.A. Payzant, C.J. Rawn, Homogeneous (co)precipitation of inorganic salts for synthesis of monodispersed barium titanate particles. *J. Mater. Sci.* **35**, 2927–2936 (2000)
- S. Dudley, T. Kalem, M. Akinc, Conversion of SiO_2 diatom frustules to BaTiO_3 and SrTiO_3 . *J. Am. Ceram. Soc.* **89**, 2434–2439 (2006)
- Y. Luo, P. Yongping, P. Zhang, J. Zhao, W. Yurong, Y. Liu, Study on dielectric properties of SiO_2 -doped BaTiO_3 ceramics. *Ferroelectrics* **492**, 10–16 (2016)
- E.P. Gorzkowski, M.J. Pan, B. Bender, C.C.M. Wu, Glass-ceramics of barium strontium titanate for high energy density capacitors. *J. Electroceram.* **18**, 269–276 (2007)
- J.S. Park, Y.H. Han, Nano size BaTiO_3 powder coated with silica. *Ceram. Int.* **31**, 777–782 (2005)
- M. Cernea, B.S. Vasile, A. Boni, A. Iuga, Synthesis, structure characterization and dielectric properties of Nb doped $\text{BaTiO}_3/\text{SiO}_2$ core-shell heterostructure. *J. Alloys Compd.* **587**, 553–559 (2014)
- Y. Zhang, M. Cao, Z. Yao, Z. Wang, Z. Song, A. Ullah, H. Hao, H. Liu, Effects of silica coating on the microstructures and energy storage properties of BaTiO_3 ceramics. *Mater. Res. Bull.* **67**, 70–76 (2015)
- K. Bi, M. Bi, Y. Hao, W. Luo, Z. Cai, X. Wang, Y. Huang, Ultrafine core-shell $\text{BaTiO}_3@/\text{SiO}_2$ structures for nanocomposite capacitors with high energy density. *Nano Energy* **51**, 513–523 (2018)
- Y. Yan, L. Liu, C. Ning, Y. Yang, C. Xia, Y. Zou, S. Liu, X. Wang, K. Liu, X. Liu, G. Liu, Improved electrical properties of SiO_2 -added BaTiO_3 ceramics by microwave sintering. *Mater. Lett.* **165**, 135–138 (2016)
- X. Lu, Y. Tong, H. Talebnezhad, J. Liu, Y. Cai, Z.Y. Cheng, L. Wang, Effects of SiO_2 coating on the dielectric and ferroelectric properties of $\text{BaTiO}_3\text{-SiO}_2$ composites, in *2017 Joint IEEE International Symposium on the Applications of Ferroelectric (ISAF)/ International Workshop on Acoustic Transduction Materials and Devices (IWATMD)/Piezoresponse Force Microscopy (PFM)*
- Q. Zhao, X. Wang, H. Gong, B. Liu, B. Luo, L. Li, The properties of Al_2O_3 coated fine-grain temperature stable BaTiO_3 -based ceramics sintered in reducing atmosphere. *J. Am. Ceram. Soc.* **101**, 1245–1254 (2018)
- H.A. Moghaddam, M.R. Mohammadi, $\text{TiO}_2\text{-BaTiO}_3$ nanocomposite for electron capture in dye-sensitized solar cells. *J. Am. Ceram. Soc.* **100**, 2144–2153 (2017)
- R. Li, Q. Li, L. Zong, X. Wang, J. Yang, $\text{BaTiO}_3/\text{TiO}_2$ heterostructure nanotube arrays for improved photoelectrochemical and photocatalytic activity. *Electrochim. Acta* **91**, 30–35 (2013)
- L. Zhang, Y. Shi, S. Peng, J. Liang, Z. Tao, J. Chen, Dye-sensitized solar cells made from BaTiO_3 -coated TiO_2 nanoporous electrodes. *J. Photochem. Photobiol., A* **197**, 260–265 (2008)
- Z.A. Garmaroudi, M.R. Mohammadi, Design of TiO_2 dye-sensitized solar cell photoanode electrodes with different microstructures and arrangement modes of the layers. *J. Sol-Gel. Sci. Technol.* **76**, 666–678 (2015)
- H. Asgari Moghaddam, M.R. Mohammadi, S.M. Seyed Reyhani, Improved photon to current conversion in nanostructured TiO_2

- dye-sensitized solar cells by incorporating cubic BaTiO₃ particles delimiting incident. *Sol. Energy* **132**, 1–14 (2016)
23. V. Paunović, L.J. Živković, V. Mitić, Influence of rare-earth additives (La, Sm and Dy) on the microstructure and dielectric properties of doped BaTiO₃ ceramics. *Sci. Sinter.* **42**, 69–79 (2010)
 24. W.H. Tzing, W.H. Tuan, H.L. Lin, The effect of microstructure on the electrical properties of NiO-doped BaTiO₃. *Ceram. Int.* **25**, 425–430 (1999)
 25. T. Nagai, K. Iijima, H.J. Hwang, M. Sando, T. Sekino, K. Niihara, Effect of MgO doping on the phase transformations of BaTiO₃. *J. Am. Ceram. Soc.* **83**, 107–112 (2000)
 26. Y. Sakabe, N. Wada, T. Hiramatsu, T. Tonogaki, Dielectric properties of fine-grained BaTiO₃ ceramics doped with CaO. *Jpn. J. Appl. Phys.* **41**, 6922 (2002)
 27. Y.H. Song, J.H. Hwang, Y.H. Han, Effects of Y₂O₃ on temperature stability of acceptor-doped BaTiO₃. *Jpn. J. Appl. Phys.* **44**, 1310 (2005)
 28. A. Shukla, R.N.P. Choudhary, A.K. Thakur, D.K. Pradhan, Structural, microstructural and electrical studies of La and Cu doped BaTiO₃ ceramics. *Physica B* **405**, 99–106 (2010)
 29. X. Cheng, M. Shen, Enhanced spontaneous polarization in Sr and Ca co-doped BaTiO₃ ceramics. *Solid State Commun.* **141**, 587–590 (2007)
 30. Y.-S. Jung, E.-S. Na, U. Paik, J. Lee, J. Kim, A study on the phase transition and characteristics of rare earth elements doped BaTiO₃. *Mater. Res. Bull.* **37**, 1633–1640 (2002)
 31. J. Li, M. Kuwabara, Preparation and luminescent properties of Eu-doped BaTiO₃ thin films by sol–gel process. *Sci. Technol. Adv. Mater.* **4**, 143–148 (2003)
 32. H. Zheng, J. Zhen-Ou, M.S. Strano, R.B. Kaner, A. Mitchell, K. Kalantar Zadeh, Nanostructured tungsten oxide—properties, synthesis, and applications. *Adv. Funct. Mater.* **21**, 2175–2196 (2011)
 33. W.J. Lee, Y.K. Fang, J.-J. Ho, W.T. Hsieh, S.F. Ting, D. Huang, F.C. Ho, Effects of surface porosity on tungsten trioxide (WO₃) films' electrochromic performance. *J. Electron. Mater.* **29**, 183–187 (2000)
 34. M.M. El-Nahass, H.A.M. Ali, M. Saadeldin, M. Zaghlol, AC conductivity and dielectric properties of bulk tungsten trioxide (WO₃). *Physica B* **407**, 4453–4457 (2012)
 35. R.S. Vemuri, K. Kamala Bharathi, S.K. Gullapalli, C.V. Ramana, Effect of structure and size on the electrical properties of nanocrystalline WO₃ films. *ACS Appl. Mater. Interfaces.* **2**, 2623–2628 (2010)
 36. Y. Slimani, M.A. Almessiere, E. Hannachi, A. Baykal, A. Manikandan, M. Mumtaz, F. Ben Azzouz, Influence of WO₃ nanowires on structural, morphological and flux pinning ability of YBa₂Cu₃O_y superconductor. *Ceram. Int.* **45**, 2621–2628 (2019)
 37. Y. Slimani, M.A. Almessiere, E. Hannachi, M. Mumtaz, A. Manikandan, A. Baykal, F. Ben Azzouz, Improvement of flux pinning ability by tungsten oxide nanoparticles added in YBa₂Cu₃O_y superconductor. *Ceram. Int.* **45**, 6828–6835 (2019)
 38. S. Rajan, P.M. Mohammed-Gazzali, G. Chandrasekaran, Electrical and magnetic phase transition studies of Fe and Mn co-doped BaTiO₃. *J. Alloys Compd.* **656**, 98–109 (2016)
 39. B. Deka, S. Ravi, A. Perumal, D. Pamu, Ferromagnetism and ferroelectricity in Fe doped BaTiO₃. *Physica B* **448**, 204–206 (2014)
 40. B.D. Cullity, *Elements of X-ray diffraction* (Addison-Wesley, Boston, 1956)
 41. E. Hannachi, Y. Slimani, A. Ekicibil, A. Manikandan, F. Ben Azzouz, Magneto-resistivity and magnetization investigations of YBCO superconductor added by nano-wires and nano-particles of titanium oxide. *J. Mater. Sci. Mater. Electron.* **30**, 8805–8813 (2019)
 42. S. Lather, A. Gupta, J. Dalal, V. Verma, R. Tripathi, A. Ohlan, Effect of mechanical milling on structural, dielectric and magnetic properties of BaTiO₃–Ni_{0.5}Co_{0.5}Fe₂O₄ multiferroic ceramics. *Ceram. Int.* **43**, 3246–3251 (2017)
 43. G. Arlt, D. Hennings, G. de With, Dielectric properties of fine-grained barium titanate ceramics. *J. Appl. Phys.* **58**, 1619–1625 (1985)
 44. S. Kappadan, T.W. Gebreab, S. Thomas, N. Kalarikkal, Tetragonal BaTiO₃ nanoparticles: an efficient photocatalyst for the degradation of organic pollutants. *Mater. Sci. Semicond. Process.* **51**, 42–47 (2016)
 45. S. Adhikari, D. Sarkar, H.S. Maiti, Synthesis and characterization of WO₃ spherical nanoparticles and nanorods. *Mater. Res. Bull.* **49**, 325–330 (2014)
 46. Y. Slimani, B. Unal, E. Hannachi, A. Selmi, M.A. Almessiere, M. Nawaz, A. Baykal, I. Ercan, M. Yildiz, Frequency and dc bias voltage dependent dielectric properties and electrical conductivity of BaTiO₃–SrTiO₃/(SiO₂)_x nanocomposites. *Ceram. Int.* **45**, 11989–12000 (2019)
 47. Y. Slimani, A. Selmi, E. Hannachi, M.A. Almessiere, A. Baykal, I. Ercan, Impact of ZnO addition on structural, morphological, optical, dielectric and electrical performances of BaTiO₃ ceramics. *J. Mater. Sci. Mater. Electron.* **30**, 9520–9530 (2019)
 48. P. Wang, C. Fan, Y. Wang, G. Ding, P. Yuan, A dual chelating sol-gel synthesis of BaTiO₃ nanoparticles with effective photocatalytic activity for removing humic acid from water. *Mater. Res. Bull.* **48**, 869–877 (2013)
 49. J.-i. Fujisawa, T. Eda, M. Hanaya, Comparative study of conduction-band and valence-band edges of TiO₂, SrTiO₃, and BaTiO₃ by ionization potential measurements. *Chem. Phys. Lett.* **685**, 23–26 (2017)
 50. Y.C. Teh, A.A. Saif, Influence of annealing temperature on structural and optical properties of sol-gel derived Ba_{0.9}Gd_{0.1}TiO₃ thin films for optoelectronics. *J. Alloys Compd.* **703**, 407–413 (2017)
 51. M. Ozta, Influence of grain size on electrical and optical properties of InP films. *Chin. Phys. Lett.* **25**, 4090–4092 (2008)
 52. L.V. Maneesha, P.V. Thomas, K. Joy, Effects of site substitutions and concentration on the structural, optical and visible photoluminescence properties of Er doped BaTiO₃ thin films prepared by RF magnetron sputtering. *Opt. Mater.* **46**, 304–309 (2015)
 53. K. Karishma, P. Ashutosh, K. Prasad, Impedance/modulus and conductivity studies on [Bi_{0.5}(Na_{1-x}K_x)_{0.5}]_{0.94}Ba_{0.06}TiO₃ (0.16 ≤ x ≤ 0.20) lead-free ceramics. *Am. J. Mater. Sci.* **6**, 1–18 (2016)
 54. A. Selmi, O. Khaldi, M. Mascot, F. Jomni, J.C. Carru, Dielectric relaxations in Ba_{0.85}Sr_{0.15}TiO₃ thin films deposited on Pt/Ti/SiO₂/Si substrates by sol–gel method. *J. Mater. Sci. Mater. Electron.* **27**, 11299–11307 (2016)
 55. T. Gopal Reddy, B. Rajesh Kumar, T. Subba Rao, J. Altaf Ahmad, Structural and dielectric properties of barium bismuth titanate (BaBi₄Ti₄O₁₅) ceramics. *Int. J. Appl. Eng. Res.* **6**, 571–580 (2011)
 56. A. Jain, A.K. Panwar, A.K. Jha, Effect of ZnO doping on structural, dielectric, ferroelectric and piezoelectric properties of BaZr_{0.1}Ti_{0.9}O₃ ceramics. *Ceram. Int.* **43**, 1948–1955 (2017)
 57. X. Dong, H. Chen, M. Wei, W. Kaituo, J. Zhang, Structure, dielectric and energy storage properties of BaTiO₃ ceramics doped with YNbO₄. *J. Alloys Compd.* **744**, 721–727 (2018)
 58. A.K. Jonscher, The 'universal' dielectric response. *Nature* **267**, 673–679 (1977)
 59. L. Singh, U.S. Rai, K. Mandal, B.C. Sin, S.-I. Leed, Y. Lee, Dielectric, AC-impedance, modulus studies on 0.5BaTiO₃–0.5CaCu₃Ti₄O₁₂ nano-composite ceramic synthesized by one-pot, glycine-assisted nitrate-gel route. *Ceram. Int.* **40**, 10073–10083 (2014)
 60. C.R. Cena, A.K. Behera, B. Behera, Structural, dielectric, and electrical properties of lithium niobate microfibers. *J. Adv. Ceram.* **5**, 84–92 (2016)

Publisher's Note Springer Nature remains neutral with regard to jurisdictional claims in published maps and institutional affiliations.